

## Article

# The Human Head Skull Role as Our First Thermoregulatory Natural Shield to Excessive Electromagnetic Fields at 1800 MHz

Miguel Á. García-Fernández <sup>1</sup>  and David A. Sánchez-Hernández <sup>2,\*</sup> 

<sup>1</sup> EMITE Ingeniería, S.L., Parcela 2.3R, Parque Tecnológico, Ctra. El Estrecho-Lobosillo km 2, E-30320 Fuente Álamo de Murcia, Spain; miguel.garcia@emite-ingenieria.es

<sup>2</sup> Universidad Politécnica de Cartagena, Antiguo Cuartel de Antigones, E-30202 Cartagena, Spain

\* Correspondence: david.sanchez@upct.es

**Abstract:** In this article, we provide concluding evidence that the human head skull acts as a first dynamic barrier to excessive electromagnetic fields (EMFs) and temperature flow at 1800 MHz. This natural barrier is designed to effectively and dynamically protect brain tissue against safety-defined threshold temperature increases due to external EMF induction. A half-wavelength dipole antenna has been employed as the EMF source. The human head is modeled by several coronal planes extracted from the Visible Human Project and combined to the exposure of a  $0.45\lambda$ -apart dipole and to heat transfer equations to accommodate for the human thermoregulatory response. The results described in this study are of great importance regarding whether thermal effects should be directly used to derive basic restrictions to EM field safety limits for human exposure. Since this study is limited to conditions under vasomotor adjustment, very excessive EMF induction may break this first natural barrier and produce excessive thermal stress, making the barrier incapable of maintaining thermal conditions on the human brain under control. This study is also limited to using a frequency of 1800 MHz.

**Keywords:** EMF dosimetry; thermoregulation; bio-heat equation; mobile communications



**Citation:** García-Fernández, M.Á.; Sánchez-Hernández, D.A. The Human Head Skull Role as Our First Thermoregulatory Natural Shield to Excessive Electromagnetic Fields at 1800 MHz. *Electronics* **2024**, *13*, 1475. <https://doi.org/10.3390/electronics13081475>

Academic Editor: Juan-Carlos Cano

Received: 11 March 2024

Revised: 10 April 2024

Accepted: 11 April 2024

Published: 12 April 2024



**Copyright:** © 2024 by the authors. Licensee MDPI, Basel, Switzerland. This article is an open access article distributed under the terms and conditions of the Creative Commons Attribution (CC BY) license (<https://creativecommons.org/licenses/by/4.0/>).

## 1. Introduction

The use of cellular mobile telecommunications systems has brought the electromagnetic fields (EMFs) emitted by these devices close to the human head, and the consequent exposure to these EMFs, i.e., its dosimetry, has been studied in depth in the literature. This was needed in order to determine which associated temperature increments could cause harmful effects on humans so as to prevent reaching those values with commercial elements. Studies have led to the discovery that an increase of more than 1 °C in any part of the brain will result in heat exhaustion or even heat stroke [1,2], and an increase of 0.2–0.3 °C in the hypothalamic region may alter thermoregulatory behavior [3]. With limits in place in terms of temperature increase, several international bodies have defined some safety margins, both for voluntary (workers) and involuntary (general public) scenarios [4] of the exposure to external EMFs that could eventually provide some temperature increase in terms of the specific absorption rate (SAR). The SAR is a measure of the rate at which radio frequency (RF) energy is absorbed by the body (in watts per kilogram), averaged over 1 or 10 g of tissue. In order to determine these safety margins, taking measurements of basic restriction values from volunteers is not always possible due to the ethical concerns regarding the implantation of deep body temperature probes and the scarcity of volunteers for such an invasive procedure. Experiments on animals are a poor approximation to the real human scenario. Using incident field extrapolation is an indirect way of protecting from excessive exposure, but the experiments published in the scientific literature to determine a thermal increase in an inner part of the human body are a rarity. One exception is Reference [5], in which exposure was generated by mobile phone (frequency 900 MHz, SAR 1.23 W/kg) in a

double-blind study performed under controlled conditions (at 24 °C and 70% humidity) with ten human volunteers. Some of these volunteers hosted a thermistor probe monitoring the tympanic temperature ( $T_{ty}$ ), each for 10 s, placed close to the aural canal membrane in the ear opposite the one in contact with a mobile phone (contralateral position). Although non-invasive in the sense of not penetrating tissue, despite being well inside the ear, the study revealed that the exposure conditions (continuous wave CW or intermittent pulsed waves PW) were a key factor to determine whether an increase in  $T_{ty}$  temperature was to be concluded. This is because on some days, the  $T_{ty}$  temperature even decreased instead of increasing with the exposure. Other studies with volunteers [6] showed contrasting results, as no reliable differences between CW and PW exposure [7] could be found. What most studies with volunteers do reveal is the fact that the human thermoregulatory system is far more advanced than that of any animal, and that human-specific studies have to be performed to address the full capacity of our thermoregulatory system when being exposed to EMFs [7]. A good overview can be seen in [7].

The inconclusive results in [5] and the contrasting findings in [6] were partially due to the fact that the human body incorporates complex thermoregulatory mechanisms which can minimize the risk of reaching these temperature increments in critical areas. Thus, several studies on the effect of EMF exposure from cellular communications systems in the human body have been performed through simulations combining Maxwell equations, thermal diffusion theory and human heterogeneous biological tissue data [8]. These attempts make diverse assumptions about both the exposure scenarios and conditions, and about the human thermoregulatory model. Most studies on the thermoregulatory mechanisms in the human body have been performed for conventional direct heating and/or cooling from external sources. Fewer studies are available on the triggering mechanisms in the thermoregulatory body caused by an external electromagnetic field (EMF) being coupled and absorbed by a close-by human body. In [9], a coarse 2 mm cell of a Japanese adult male was used along with some approximation through heating factors, defined as the increase in temperature in the steady state per unit of exposure, and static SAR values to determine minute temperature increases in the human skin. An adult model and 7-year-old child model with only five tissues were used in [10] to determine the thermal effects of exposure to a 5 W transmission at 900 MHz of a patch antenna and three different usage patterns. Thermal properties were also assumed to be constant and despite simulated SAR values being higher than those defined in safety standards, the associated temperature increase in both the adult and the child were not found to overpass the damaging thresholds. Slightly higher increments were found in the child compared to the adult. A more recent overview of EMF exposure above 6 GHz with thermoregulation can be found in [11]. In [11], a vast analysis of the literature revealed that there is a very large amount of uncertainty associated with the variability within human individuals of several key variables in the studies. These variables include dielectric and thermal properties of tissues, physiological and anatomical variability, something nearly unexplored, or skin blood thermoregulatory reaction to EMFs. These factors led to up to a 10-fold increase or decrease in the results and called for quantifying these uncertainties to improve the rationale of the limits in the international guidelines/standards.

The evaluation of compliance with safety limits is, therefore, usually accomplished by measuring the SAR with automated systems and homogeneously filled phantoms, that is, with robots and artificial materials. This has led to large overestimation of margins set on limits, since the human body is heterogeneous in nature with several additional and complex minimizing elements like thermoregulation. Today, it is clear that the SAR alone does not provide an adequate description of the regional thermal environment in this problem [12], and while several correction factors have been proposed to overcome this [13,14], they have also proven to be erroneous for modern cellular telecommunications systems antennas [15]. In these modern communications systems, specific technology-related parameters like the frequency range, the duty cycle, or the antenna topology

cannot be separated from the specific heterogeneous human tissue structure receiving exposure [16].

In this work, a combined Maxwell–thermal transfer model has been developed and used to demonstrate that the human head acts as a first barrier, protecting us against potential damage from exposure to EMFs at 1800 MHz. The inherent protection is shown to be due to the head tissue structure and its thermoregulatory capacity, and particularly due to the skull’s role in this structure. This frequency is commonly used for current GSM (2G) [17], WCDMA (3G) [18], LTE (4G) [19] and New Radio (5G) [20] FR1 cellular technologies. This initial protection, with our skull helping to avoid thermal damage of most sensible brain tissues, keeps the subject safe against overheating processes while in the thermopreferendum region. While diverse studies exist on the potential long-term non-heating effects of low-level exposure to electromagnetic fields, this manuscript solely considers heating effects, as they drive the current protection standards against the human exposure to electromagnetic fields. The diverse simulations show that this protective nature of the skull is achieved by the combination of our specific tissue layer structure and the specific position and thermal characteristics of the skull. The results also show that substituting the skull with metal prosthetic elements, which happens in some surgery procedures, has a tremendous effect on breaking this natural protective barrier. This is reported here for the first time. With respect to using commercial codes or Transmission Line Matrix (TLM) techniques, the developed method saves considerable time and memory in achieving the same accuracy of 0.05 °C of other methods, using a cell size of 500  $\mu\text{m}$  instead of 62.5  $\mu\text{m}$  to achieve this.

In Section 2, the different materials and methods employed are described. Section 3 includes a validation of the employed method and the simulated results and a discussion on the results. Finally, Section 4 contains the conclusions, including the main findings of this study and future research lines. A list of references is also provided.

## 2. Materials and Methods

The electrical and thermal properties of the employed tissues have been extracted from the literature [21]. The employed biological data are reproduced in Table 1. The 3D head model and some relevant coronal planes are from the Visible Human Project, as depicted in Figure 1 [22].

**Table 1.** Electrical and thermal properties used in the simulations.

Tissue	$\epsilon_r$	$\sigma$ (S/m)	$\rho$ Density (kg/m <sup>3</sup> )	C Specific Heat Capacity (J/kg·°C)	K Thermal Conductivity (W/m·°C)	A Metabolic Heat Production (W/m <sup>3</sup> )	B Blood Flow Associated Term (W/m <sup>3</sup> ·°C)
Blood	59.37	2.044	1058	3840	0.49	0	0
Blood Vessel	43.34	1.066	1040	3553	0.46	1600	9000
Bone (Cancellous)	19.34	0.588	1920	2150	0.30	2510	14,120
Bone (Cortical)	11.78	0.275	1990	1650	0.30	0	0
Bone (Marrow)	5.37	0.069	1040	2700	0.22	5020	28,230
Brain (Cerebellum)	46.11	1.709	1038	3687	0.57	10,040	56,490
Brain (Gray Matter)	50.08	1.391	1038	3687	0.57	10,040	56,490
Brain (White Matter)	37.01	0.915	1038	3600	0.50	2820	15,890
Skin	38.87	1.845	1125	3610	0.42	2190	12,310

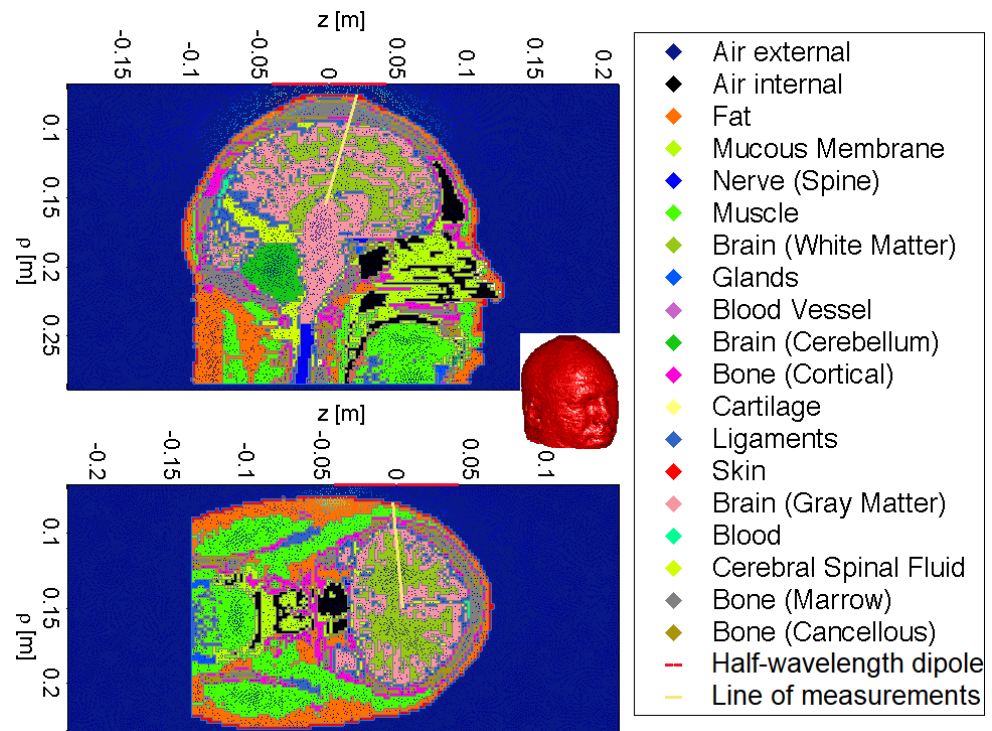


**Figure 1.** 3D view of the human head model (**top-left**), legend of tissues (**middle**), top cranial slice (**bottom left**) and schema used in this manuscript (**right**) in which the line of measurements is depicted in light yellow and the z-oriented dipole in light red and centred at the origin of coordinates ( $\rho = 0, z = 0$ ).

For reproducibility, we have employed the EMF produced by a half-wavelength dipole antenna at 1800 MHz as the field source. The power radiated by the dipole was modified so as to provide a maximum temperature increase of  $0.2\text{ }^{\circ}\text{C}$  in the skull–brain borderline. The above is carried out in two different time scales corresponding to exposures of 6 and 30 min. In order to analyze the efficiency of the head layer structure, many different head regions have been considered: over the top of the cranium, from the back of the head, and from several positions near and in front of both of the ears, both of the eyes and both of the temples. The Visible Human Project slices for these regions are illustrated in Figure 1. The distance between the dipole antenna and the human head is fixed once and for all to  $0.45\lambda$  in a position near to the ear reference point (ERP). The center of the dipole was settled as the origin of coordinates. At this distance, the heterogeneous human head model matches the dipole antenna impedance in the initial setting, which represents a worst-case scenario for induced heating and triggering thermoregulatory actions, causing the highest possible SAR and temperature increase for a given antenna output power. The resulting mathematical model is studied by an in-house integration of Maxwell equations and heat transfer equations to accommodate for the human thermoregulatory response to the exciting EMF exposure. The differential equation that models the above-described system is usually called the bio-heat equation, and it is a refinement of the original model used by Pennes [23]. The methodology in [23] was used for the thermal evaluation using the bio-heat equation. This differential equation incorporates the electromagnetic and heat diffusion data applied to human tissue by,

$$\rho \cdot C \cdot \frac{\partial T}{\partial t} = \nabla \cdot (K \cdot \nabla T) + \rho \cdot SAR + A + B \cdot (T_b - T) \quad (1)$$

where  $C$  is the specific heat capacity,  $K$  is the thermal conductivity,  $\rho$  is the mass density of the tissue,  $A$  is the metabolic heat production,  $B$  is the heat-sink strength,  $T_b$  is the blood temperature,  $t$  is time, and  $T$  is the temperature. The first task in solving the above

equations is to obtain the SAR on each individual layer. Its value can be defined from knowledge of the corresponding root mean square (RMS) value of the electric field  $E$  using the well-known equation,

$$SAR = \frac{\sigma \cdot E^2}{\rho} \quad (2)$$

where  $\sigma$  is the electrical conductivity of the tissue. Once the SAR is obtained, it can be inserted into the modified bio-heat equation. Finally, the above set of equations is fed with the necessary boundary data by,

$$K \cdot \hat{n} \cdot \nabla T = H \cdot (T_r - T) \quad (3)$$

where  $(\hat{n}, H, T_r)$  stand for the normal unit vector to the boundary of the human head, the environment heat transfer coefficient and the room temperature, respectively. In order to find the solution, an in-house software code was prepared in combination with the Partial Differential Equation (PDE) toolbox in MATLAB, by which linear static analyses for structures including deformation, stress, and strain can be computed in combination with a direct integration solver for modeling structural dynamics and vibration. This allows for the analysis of a component's structural characteristics to find natural frequencies and mode shapes as well as modeling conduction-dominant heat transfer problems to calculate temperature distributions, heat fluxes, and heat flow rates through surfaces. A MATLAB code was programmed to be able to introduce a dipole with any length as the EMF source to the problem.

After the SAR is calculated, the temperature increase is evaluated for all tissues by solving the modified bio-heat Equation (1), where  $T_b$  is set to 37 °C. The boundary conditions were established, with  $H$  equal to 7 W/(m<sup>2</sup>·°C) and a room temperature of 23 °C. Room temperature was chosen to follow within the thermopreferendum region. In this region, a lightly clothed man would feel comfortable sedentary in still air [24]. The in-house thermal model includes heat diffusion and convection, metabolic heat production and heat-sink from tissue volume by blood perfusion. Thermoregulatory control can be achieved in the head model in real time, which can keep a constant temperature under no RF exposure, being slightly altered by the heat loss in body surface due to intimate contact to air. Thermal conditions in this contribution are kept just under the vasomotor adjustment, that is, just under the lower critical temperature (LCT) [25]. This facilitates the use of basal metabolism as adequate. In this way, no vaporization is evaluated and harsh electromagnetic exposure is out of the scope for this contribution, that is, mass transfer and their associated heat-transfer mechanisms are avoided. Once the coronal plane is identified and we have the corresponding temperature increase on any point of it, we localize the spot in the brain of maximal increase in temperature  $p$ . Then, we define our line of measurements  $\overline{cp}$  as the line that begins at the geometrical center of the brain  $c$  and passes through  $p$  ending on the aerial region, as shown in Figure 1. Our simulated results and data are displayed along this linear axis. In this way, given a particular antenna-head configuration, we define a particular axis that passes throughout the point of maximum heating that permits us to control the most vulnerable part of the brain.

### 3. Simulated Results and Discussion

In order to validate the developed code, Figure 2 depicts the temperature distribution in a 1 mm wide Plexiglas Petri dish. The dish contains water that is heated up by an EMF source [26]. The temperature results in [26,27] with an XLIM code for a uniform mesh with cell sizes of 500, 250, 125, 62.50 and 31.25 μm are reproduced in Figure 2. Figure 2 also shows temperature results calculated with the developed in-house software of this manuscript, with a triangular mesh with maximum cell sizes of 1 mm, 500 μm, 250 μm and 125 μm. It can be observed from Figure 2 that the XLIM code needs a cell size of 62.50 μm to achieve accurate results. A maximum cell size of 500 μm is enough with the MATLAB code to achieve the same accuracy, which considerably reduces memory and computational time.

An accuracy of  $0.05\text{ }^{\circ}\text{C}$  was selected for the simulations to validate the proposal, which was well validated against [26,27], and a  $500\text{ }\mu\text{m}$  cell size was selected.

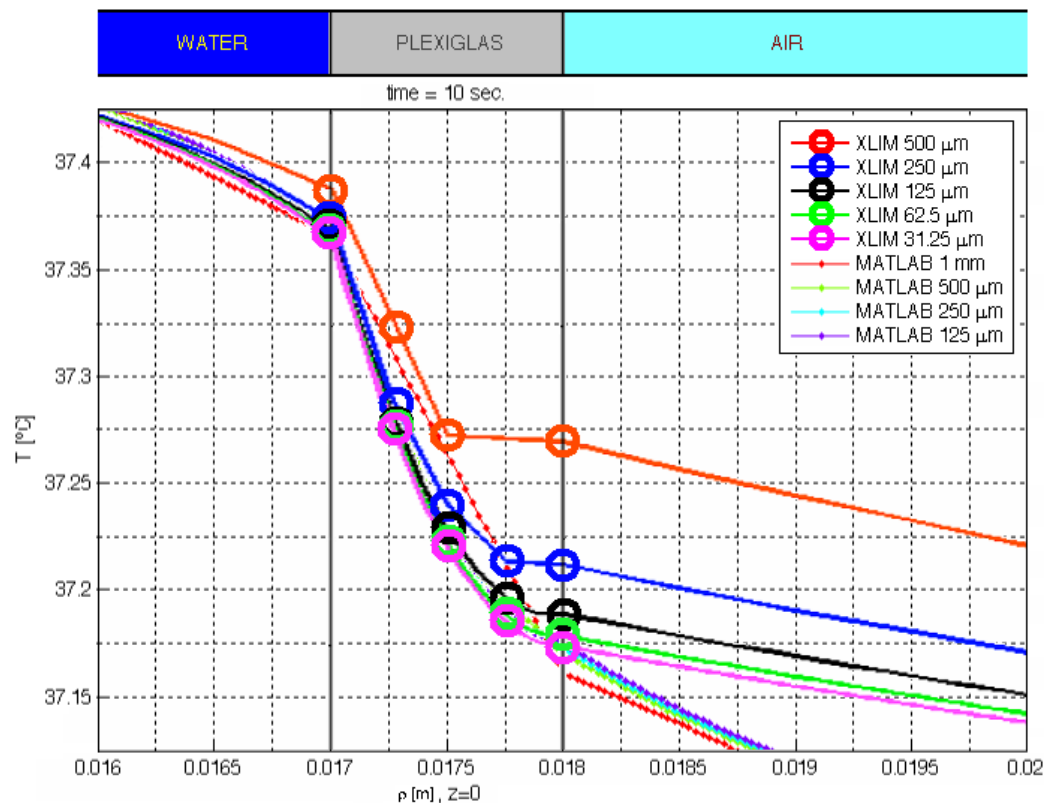


**Figure 2.** Simulated temperature after 10 s of exposure with SAR = 200 W/kg.

The results are expressed in terms of minimal power delivered and the associated SAR required to produce the aimed maximum local increment of brain tissue of  $0.2\text{ }^{\circ}\text{C}$  in different scenarios. This is currently set as the maximum incremental value in the hypothalamus region for human safety. In addition, different figures of local temperature increments along the different tissues of the brain are provided. To test our working hypothesis, i.e., that the head multilayer structure acts as a thermoregulatory first barrier to excessive EMF dosimetry, we probed the human head model to the radiation of the dipole antenna from different positions in the vicinity of the head. Following the procedure described in the previous section, we obtained the increase in temperature along the  $\bar{c}\bar{p}$  axis for each one of the different configurations under study. The delivered power of the antenna was tuned to produce a maximal increment of temperature at a  $p$  of  $0.2\text{ }^{\circ}\text{C}$ . The above was simulated for short and long exposure corresponding to 6 min and 30 min, respectively. In this way, we devised a procedure to capture the strength of the natural protection of the head multilayer structure at the diverse time averaging periods defined in the standards worldwide.

The same overall behavior is shown in all of the different analyzed points. Results for the top cranial and right temple regions from the skin to the center of the head are depicted in Figures 3 and 4, respectively, in which a 2D cut of the thermal simulated result through a line from the top cranial (Figure 3) and right temple (Figure 4) to the center of the head is made. It is in these regions in which we observe the highest outer regions temperature increase. The figures also include a brown vertical line to identify the start of the bone tissue (skull) and a blue vertical line to identify the start of the brain tissue, as well as the incident electric field at the skin on the outside and in its inside parts, this last one being that which ultimately causes the SAR values in tissues. In the simulation figures, the same tissue color code as that in Figure 1 is followed. All simulations are carried out for both 6

and 30 minutes, and the delivered power to the head is identified in the trace label. From these figures, it is clear that almost no thermal fluctuations or SAR leaks into the inner brain. Most of the energy absorbed by the head is localized in the outer region outside the skull. As expected, the time dependence of the above phenomena shows a conformal behavior, since only the relative power needs to be re-scaled to recover the correct curves. This reinforces our aim to maintain the experiments just below the LCT region.

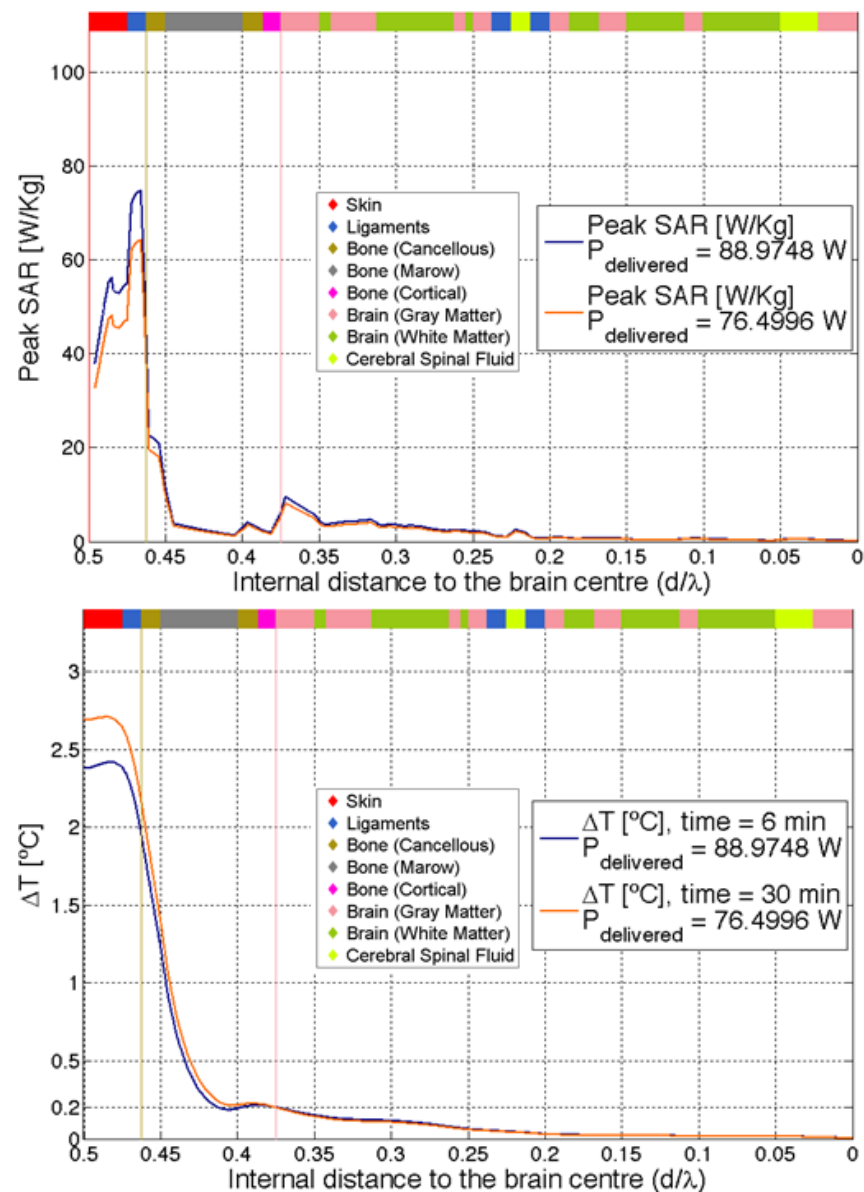


**Figure 3.** SAR (up) and temperature increase (down) for the cranial setting. E-field values at skin-outside and skin-inside were 689.10 and 152.10 V/m, respectively, for an exposure of 6 min.

The results show that the outer layers of the human head constitute a built-in first barrier to EMF induction from external sources, which acts as a dynamical barrier, scattering thermal fluctuations and EMFs away from the brain back to the external regions. In this dynamical process, the un-scattered thermal fluctuations and the EMFs that reach the brain tissue are really subdominant, where the ratio of scattered to transmitted thermal fluctuations is only of order  $10^{-3}$ . In the above data analyses, it is not difficult to identify the location of this natural first barrier as the region where the thermal fluctuations and EMFs decay abruptly. In all performed simulations, we found that this region corresponds to the location of the skull or its natural continuation. This corresponds to the region delimited

by the vertical brown or pink lines in Figures 3 and 4. In consequence, it can be observed that the principal component of the natural shield is indeed the multilayer head structure, which makes the skull properties and the specific position of the skull within the multilayer tissue structure essential to this discovered initial protective nature.

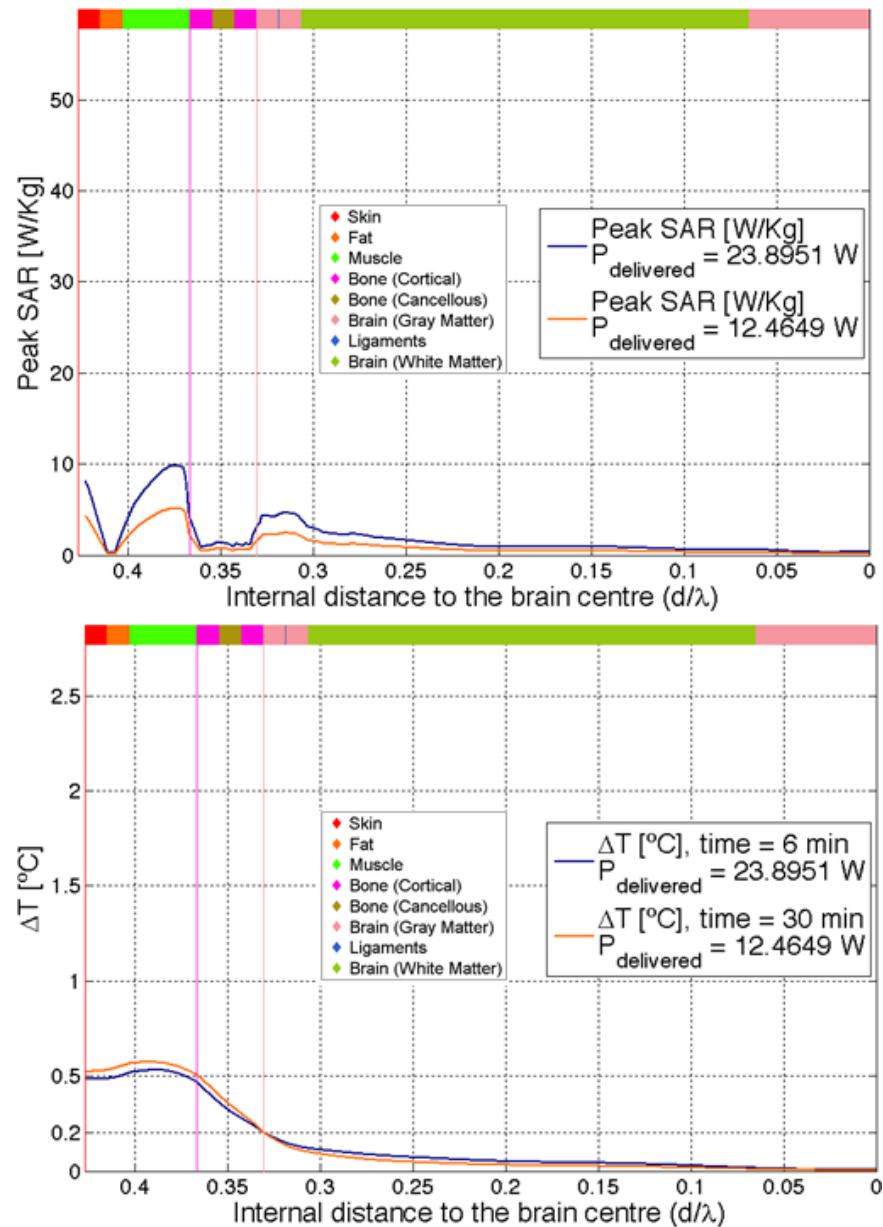


**Figure 4.** SAR (up) and temperature increase (down) for the temple setting. E-field values at skin outside and skin inside were 357.11 and 70.50 V/m, respectively, for an exposure of 6 min.

Since this represents an important finding, to cross-check the above results, we have considered the case of skull-less heads, where the bones are replaced by a layer of less thermally efficient brain tissue. While this is not a typical surgical procedure for diverse illnesses, this putative head would have no mechanical protection, but it makes theoretical sense, since we are only interested in its thermodynamical response to EMF exposure from an external source. This could then be used to compare and discuss the effect of using different non-bone materials instead of the skull. Results for the same 2D cuts in Figures 3 and 4 but with this change replacing the skull with a less-efficient thermal tissue are shown in Figures 5 and 6. The results confirm our hypothesis again. From Figures 5 and 6, we can observe that the clear cut defining the shield region in Figures 3 and 4 cannot be found.

The results also show a very poor efficiency when compared to Figures 3 and 4. It is also noticeable that much less delivered power is needed to achieve the safety limit increment of  $0.2\text{ }^{\circ}\text{C}$  in brain tissues.

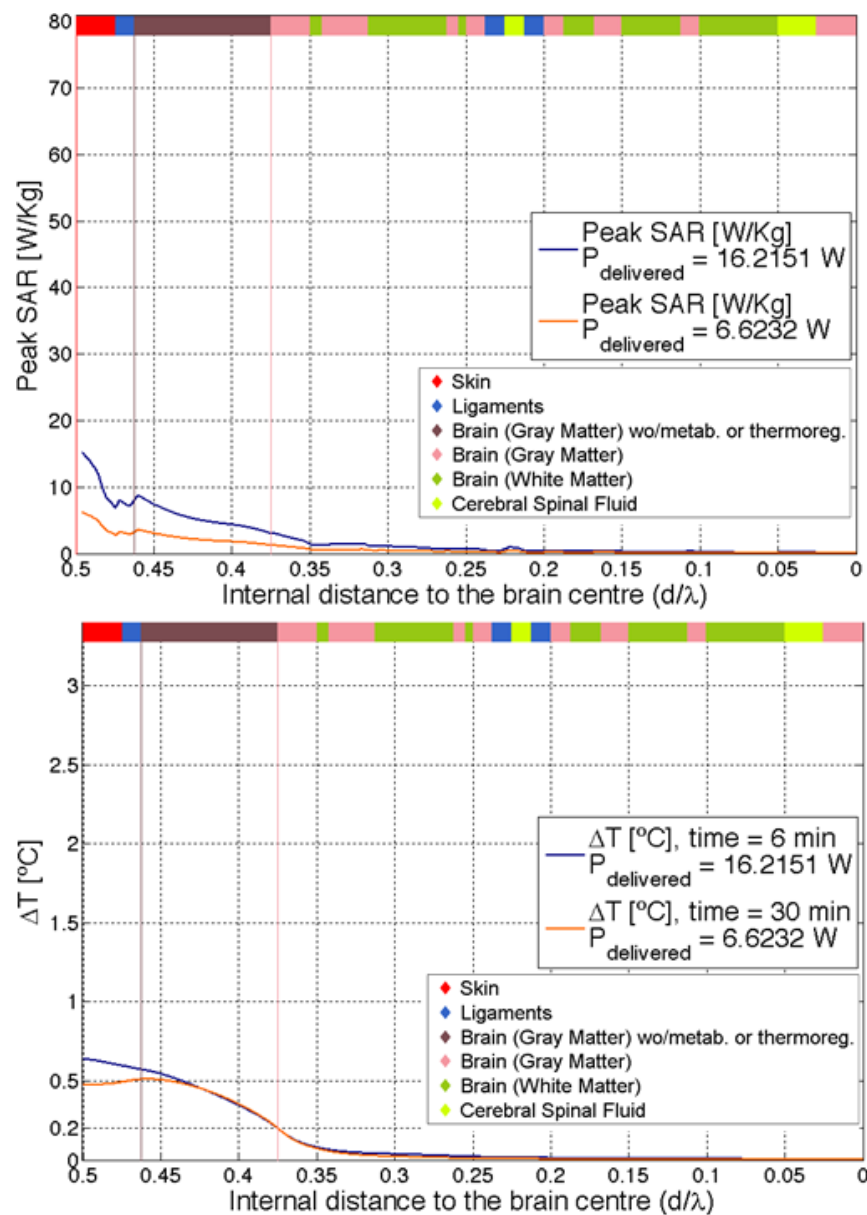


**Figure 5.** SAR (up) and temperature increase (down) for the cranial setting without the skull. E-field values at skin outside and skin inside were 294.18 and 96.57 V/m, respectively, for an exposure of 6 min.

But the less-efficient skull is not a real situation, and it could not be used to derive substantial conclusions. Thus, the study engaged in covering the possibility of having other real materials taking the place of the skull to effectively observe the skull performance. We then added artificial skulls made of aluminum or copper as other exposure scenarios. This selection was made based on the fact that metallic implants with biocompatible materials are now commonplace, and while the newly defined heads with metallic implants are not realistic, they are useful for comparing their thermodynamical behavior. Since some metal alloys have a high thermal conductivity and a mechanical resistance similar to the skull, the differences could only be attributed to their different behavior against electromagnetic field exposure. The results are illustrated in Figures 7 and 8. From Figures 7 and 8, it

can be observed that there is a clear barrier behavior, similar to the one found innately in Figures 3 and 4 with the bone skull. There are general similarities and some differences in the response to the power and exposure time when compared to the natural skull. In general, copper is better behaved for short exposure in opposition to long exposure, which is due to its high thermal conductivity, and a significant difference can be considered in the standards for long-term exposure scenarios. Nevertheless, these results are complementary and serve only to narrow our conclusion that the natural head multilayer structure acts as a natural first barrier against excessive EMF exposure from external sources, and, therefore, also against potentially dangerous increased thermal flow within the human brain. In fact, the natural skull, in conjunction with the multilayer structure of the head, seems to be very efficient and a key factor for protection compared to their metallic un-natural counterparts.

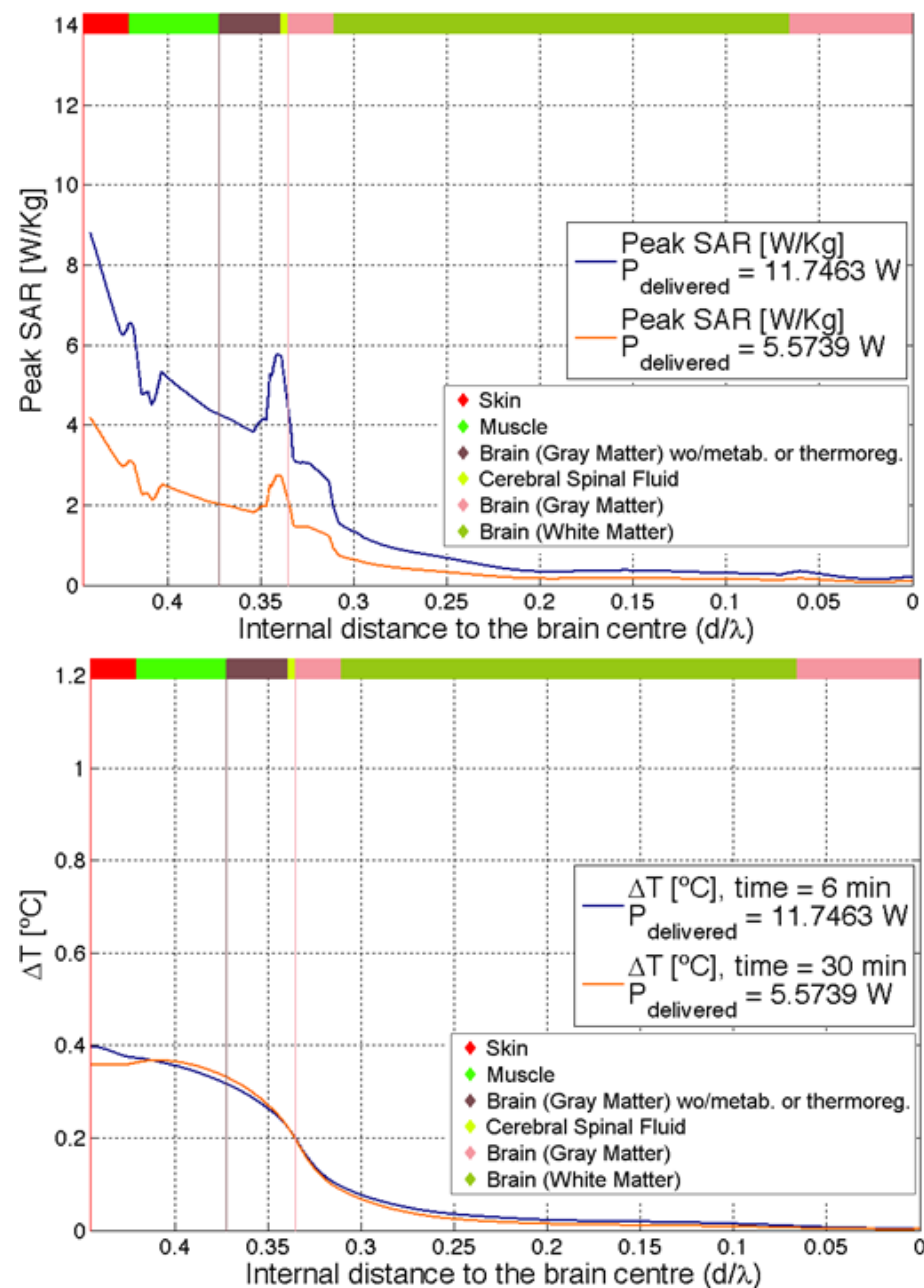


**Figure 6.** SAR (up) and temperature increase (down) for the temple setting without the skull. E-field values at skin outside and skin inside were 250.38 and 73.27 V/m, respectively, for an exposure of 6 min.

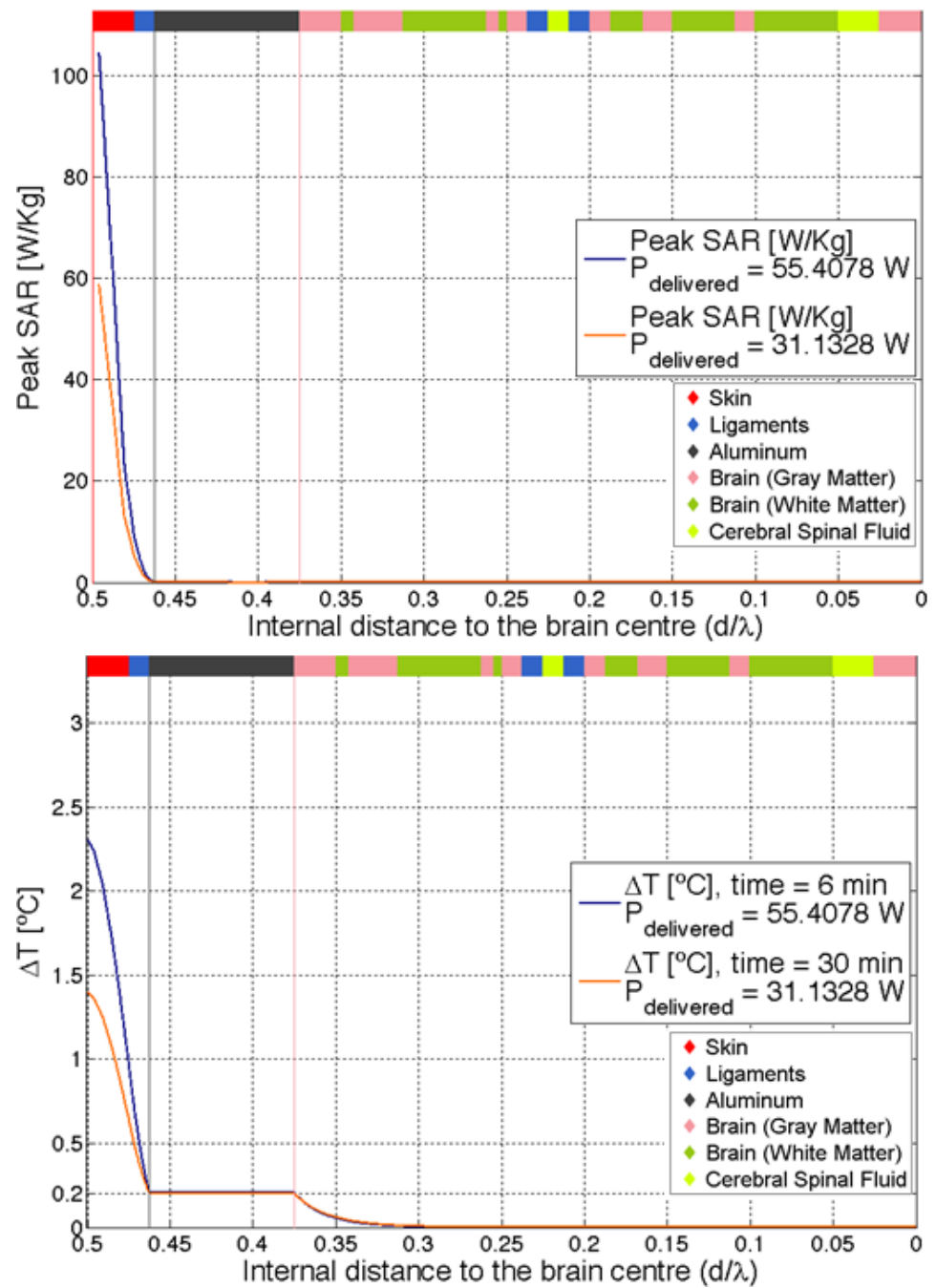
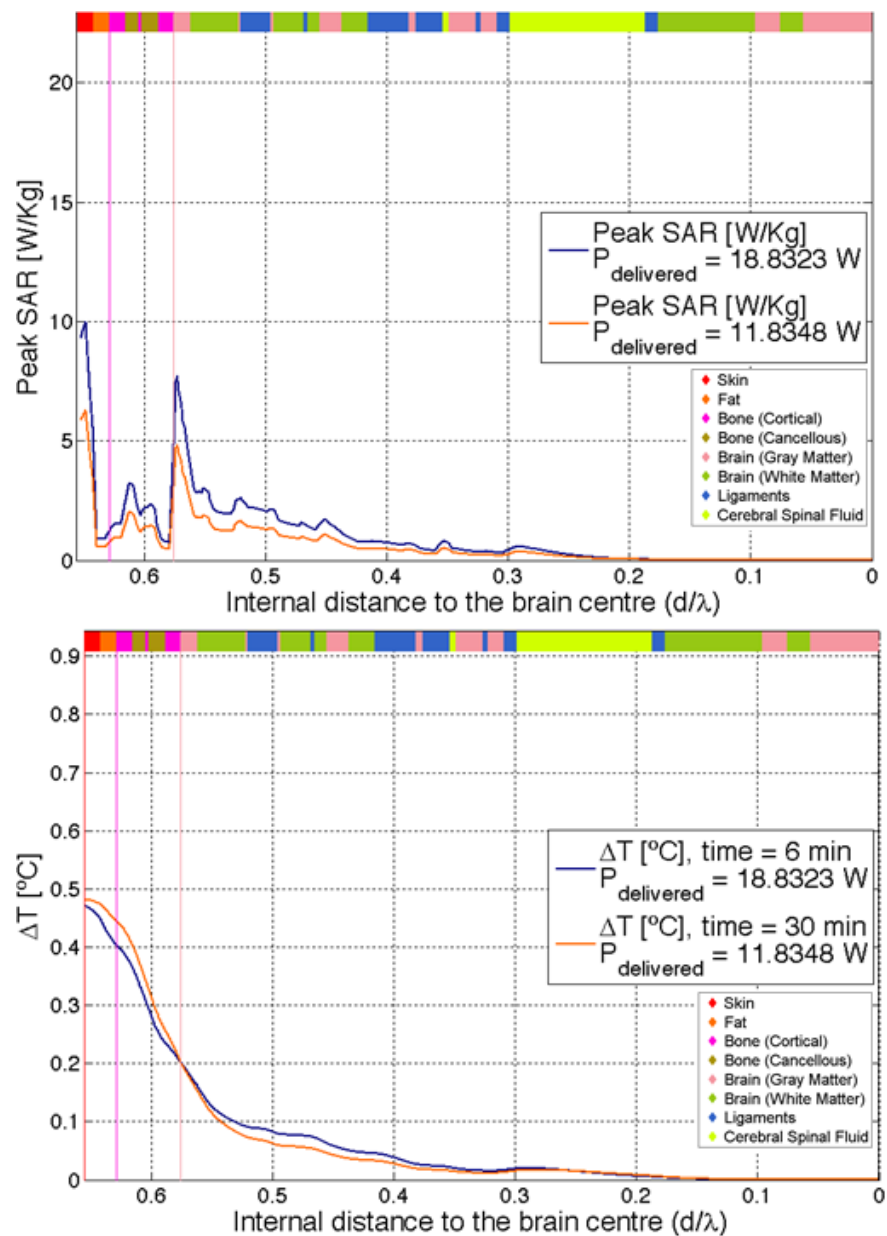


**Figure 7.** SAR (up) and temperature increase (down) for the cranial setting with no skull but aluminium. E-field values at skin outside and skin inside were 543.79 and 252.47 V/m, respectively, for an exposure of 6 min.



.05

**Figure 8.** SAR (up) and temperature increase (down) for the temple setting with no skull, but aluminium. E-field values at skin outside and skin inside were 317.03 and 75.42 V/m, respectively, for an exposure of 6 min.

#### 4. Conclusions

In this article, we have used a realistic human head model exposed to EMFs, employing a hybrid framework based on electromagnetic field theory, heat transport theory and thermoregulatory response of the human body. The specific position and properties of the skull within the human head and its multilayer structure have been identified to act as an initial protective structure, preventing external electromagnetic fields and their associated thermal increase from getting into the inner brain. The natural electromagnetic barrier also seems to act as a thermo-insulator, since it warms up as much as the outer tissue but keeps the temperature gradient in the brain small and within safe margins. Therefore, we can conclude that we are in the presence of a natural and dynamic electromagnetic and thermal initial barrier that protects our brain to non-harsh EMF exposure. This conclusion is to be made with consideration of its limitations, due to the range of parameters analyzed in this research together with the simplifications involved in the modeling of a realistic

human head. The main limitation of this study is that the findings are valid only under the vasomotor adjustment with no sweating, so the protective nature is limited to the capabilities of our thermoregulatory system. The limits to the inherent protective nature of the skull against EMF could be found with future studies in the region after the avalanche effect happens, something that is very challenging. In particular, there are many factors to be accounted for in the employed thermoregulatory model, such as sweating, panting, variable heat loss in lungs, capillarity, vasodilatation, variable blood flow or metabolism, clothing, circadian rhythm or even alterations in the thermoregulatory response itself due to temperature increases in the hypothalamus provided by the deposited RF energy, etc. With the powerful computing resources available today, however, it is not risky to envisage the possibility of reducing current scientific uncertainties regarding human exposure to electromagnetic fields using the human thermal response. The use of hybrid models brings new possibilities to deliver more accurate basic restrictions to these safety levels. The adoption of a basic restriction directly involving a temperature increase with different reference levels for various parts of the body according to their sensitivity to heat, in combination with the existing SAR-based limits, would bring more precise data for the human EMF exposure scenario, which in view of the presented results, may certainly have to be frequency-dependent in a less coarse way. The fact that some metal implants may provide a less efficient protective barrier in the long term than the natural skull could have a significant impact in some surgical procedures and safety standards. Future research will include the determination of the avalanche effect that breaks the protective nature of the head, which may be strongly dependent upon the employed thermoregulatory model, as well as extending the study to more recently available New Radio Frequency Range 2 (NR FR2) mm wave cellular frequencies [27,28].

Likewise, the effect on the protective nature of the skull against EMF exposure when implanting deep brain stimulation (DBS) neuroprosthesis, when running MRI scans in patients with heart pacemakers, when using cardioverter defibrillators metallic leads under RF pulsation, or the effect of hydrocephalous valves when subjected to EMF exposure from mobile phones, among many other surgical and treatment procedures, can be studied using this method.

**Author Contributions:** Writing—original draft, M.Á.G.-F. and D.A.S.-H.; Writing—review & editing, M.Á.G.-F. and D.A.S.-H. All authors have read and agreed to the published version of the manuscript.

**Funding:** This research was funded by EMITE Ingeniería, S.L.

**Data Availability Statement:** Data are contained within the article.

**Acknowledgments:** The authors are particularly grateful to those who have also contributed to some extend to this article, in particular to Marylène Cueille and Philippe Lévêque. The authors would like to acknowledge the funding from EMITE Ingeniería, S.L.

**Conflicts of Interest:** Author Miguel Á. García-Fernández was employed by the company EMITE Ingeniería, S.L. The remaining authors declare that the research was conducted in the absence of any commercial or financial relationships that could be construed as a potential conflict of interest.

## References

1. International Commission on Non-Ionizing Radiation Protection (ICNIRP) Guidelines. Guidelines for limiting exposure to time-varying electric, magnetic, and electromagnetic fields (up to 300 GHz). *Health Phys.* **1998**, *74*, 494–522.
2. American Conference of Government Industrial Hygienists (ACGIH). *Threshold Limit Values (TLVs) for Chemical Substances and Physical Agents and Biological Exposure Indices (BEIs)*; American Conference of Governmental Industrial Hygienists (ACGIH): Cincinnati, OH, USA, 1996.
3. Adair, E.R.; Adams, B.W.; Akel, G.M. Minimal changes in hypothalamic temperature accompany microwave-induced alteration of thermoregulatory behavior. *Bioelectromagnetics* **1984**, *5*, 13–30. [[CrossRef](#)] [[PubMed](#)]
4. IEC 62209-1; Human Exposure to Radio Frequency Fields from Hand-Held and Body-Mounted Wireless Communication Devices—Human Models, Instrumentation, and Procedures—Part 1: Procedure to Determine the Specific Absorption Rate (SAR) for Hand-Held Devices Used in Close Proximity to the Ear (Frequency Range of 300 MHz to 3 GHz). International Electrotechnical Commission: Geneva, Switzerland, 2005.

5. Bortkiewicz, A.; Gadzicka, E.; Szymczak, W.; Zmysłony, M. Changes in tympanic temperature during the exposure to electromagnetic fields emitted by mobile phone. *Int. J. Occup. Med. Environ. Health* **2012**, *25*, 145–150. [[CrossRef](#)] [[PubMed](#)]
6. Kodera, S.; Hirata, A.; Funahashi, D.; Watanabe, S.; Jokela, R.J. Temperature rise for brief radio-frequency exposure below 6 GHz. *IEEE Access* **2018**, *6*, 65737–65746. [[CrossRef](#)]
7. Adair, E.R.; Black, D.R. Thermoregulatory Responses to RF Energy Absorption. *Bioelectromagnetics* **2003**, *6*, 17–38. [[CrossRef](#)] [[PubMed](#)]
8. Bernardi, P.; Cavagnaro, M.; Pisa, S.; Piuze, E. SAR Distribution and Temperature Increase in an Anatomical Model of the Human Eye Exposed to the Field Radiated by the User Antenna in a Wireless LAN. *IEEE Trans. Microw. Theory Tech.* **1998**, *46*, 1118–1126. [[CrossRef](#)]
9. Kodera, S.; Gomez-Tames, J.; Hirata, A. Temperature elevation in the human brain and skin with thermoregulation during exposure to RF energy. *Biomed. Eng.* **2018**, *17*, 1. [[CrossRef](#)] [[PubMed](#)]
10. Bhargava, D.; Leeprechanon, N.; Rattanadecho, P.; Wessapanet, T. Specific absorption rate and temperature elevation in the human head due to overexposure to mobile phone radiation with different usage pattern. *Int. J. Heat Mass Transf.* **2019**, *130*, 1178–1188. [[CrossRef](#)]
11. Hirata, A.; Kodera, S.; Sasaki, K.; Gomez-Tames, J.; Laakso, I.; Wood, A.; Watanabe, S.; Foster, K.R. Human exposure to radiofrequency energy above 6 GHz: Review of computational dosimetry studies. *Phys. Med. Biol.* **2021**, *66*, 08TR01. [[CrossRef](#)] [[PubMed](#)]
12. Mason, P.A.; Hurt, W.D.; Walters, T.J.; D’Andrea, J.A.; Gajšek, P.; Ryan, K.L.; Nelson, D.A.; Smith, K.I.; Ziriac, J.M. Recent advances in dosimetry measurements and modeling. In *Radio Frequency Radiation Dosimetry*; Klauenberg, B.J., Miklavčič, D., Eds.; Springer: Dordrecht, The Netherlands, 2000; pp. 141–155.
13. Ghandi, O.P.; Lazzi, G.; Furse, C.M. Electromagnetic absorption in the human head and neck for mobile telephones at 835 and 1900 MHz. *IEEE Trans. Microw. Theory Tech.* **1996**, *44*, 1865–1873.
14. CENELEC EN50383; Basic Standard for the Calculation and Measurement of Electromagnetic Field Strength and SAR Related to Human Exposure from Radio Base Stations and Fixed Terminal Stations for Wireless Telecommunication Systems (110 MHz–40 GHz). European Committee for Electrotechnical Standardization: Brussels, Belgium, 2002.
15. Joseph, W.; Martens, L. Safety factor for determination of occupational electromagnetic exposure in phantom model. *Electron. Lett.* **2003**, *39*, 1663–1664. [[CrossRef](#)]
16. Christ, A.; Klingenbock, A.; Samaras, T.; Goiceanu, C.; Kuster, N. The dependence of electromagnetic far-field absorption on body tissue composition in the frequency range from 300 MHz to 6 GHz. *IEEE Trans. Microw. Theory Tech.* **2006**, *54*, 2188–2195. [[CrossRef](#)]
17. 3GPP TS 45.005 V17.0.0 (2022-03); Technical Specification 3rd Generation Partnership Project; Technical Specification Group Radio Access Network; GSM/EDGE Radio Transmission and Reception (Release 17). 2022.
18. 3GPP TR 25.889 V6.0.0 (2003-06); Technical Report 3rd Generation Partnership Project; Technical Specification Group Radio Access Network; Feasibility Study Considering the Viable Deployment of UTRA in Additional and Diverse Spectrum Arrangements. 2003.
19. 3GPP TS 36.10 V18.4.0 (2024-01); Evolved Universal Terrestrial Radio Access (E-UTRA); User Equipment (UE) Radio Transmission and Reception. 2024.
20. 3GPP TS 38.101-1 V18.4.0 (2023-12); Technical Specification 3rd Generation Partnership Project; Technical Specification Group Radio Access Network; NR; User Equipment (UE) Radio Transmission and Reception; Part 1: Range 1 Standalone (Release 18). 2023.
21. Gabriel, C. *Compilation of the Dielectric Properties of Body Tissues at RF and Microwave Frequencies*; Brooks Air Force Tech. Rep.; AL/OE-TR-1996-003.7; 1996.
22. Ackerman, M.J. The Visible Human Project. *Proc. IEEE* **1998**, *86*, 504–511. [[CrossRef](#)]
23. Pennes, H.H. Analysis of tissue and arterial blood temperature in the resting human forearm. *J. Appl. Physiol.* **1948**, *1*, 93–122. [[CrossRef](#)] [[PubMed](#)]
24. Durney, C.H.; Massoudi, H.; Iskander, M.F. *Radiofrequency Radiation Dosimetry Handbook*, 4th ed.; Brooks Air Force Base; TX 78235-5301 Tech. Rep. USAFSAM-TR-85-73; 1996.
25. Adair, E.R.; Kelleher, S.A.; Mack, G.W.; Morocco, T.S. Thermophysiological responses of human volunteers during controlled whole-body ratio frequency exposure at 450 MHz. *Bioelectromagnetics* **1998**, *19*, 232–245. [[CrossRef](#)]
26. Cueille, M.; Makhlof, O.; Dubard, J.-L. TLM computation of temperature distribution in human head exposed to electromagnetic waves. In Proceedings of the IEEE International Symposium on Antennas and Propagation (APSURSI), Fajardo, PR, USA, 26 June–1 July 2016.
27. Joubert, V.; Leveque, P.; Cueille, M.; Bourthoumieu, S.; Yardin, C. No apoptosis is induced in rat cortical neurons exposed to GSM phone fields. *Bioelectromagnetics* **2006**, *28*, 115–121. [[CrossRef](#)] [[PubMed](#)]
28. Cueille, M.; Makhlof, O.; Dubard, J.-L. A new TLM algorithm to solve the Pennes’s equation for dosimetry applications. In Proceedings of the European Microwave Conference (EuMC), Paris, France, 7–10 September 2015.

**Disclaimer/Publisher’s Note:** The statements, opinions and data contained in all publications are solely those of the individual author(s) and contributor(s) and not of MDPI and/or the editor(s). MDPI and/or the editor(s) disclaim responsibility for any injury to people or property resulting from any ideas, methods, instructions or products referred to in the content.